Acta Cryst. (1987). B43, 49-56

Incommensurate Superstructures and Phase Transition of Strontium Barium Niobate (SBN)

BY L. A. BURSILL AND PENG JU LIN

School of Physics, University of Melbourne, Parkville, Victoria 3052, *Australia*

(*Received* 12 *August* 1985; *accepted* 24 *July* 1986)

Abstract

The superstructures exhibited by ferroelectric strontium barium niobate (SBN; $Sr_{0.5}Ba_{0.5}Nb_2O_6$) have been studied by electron diffraction throughout the temperature range $93 < T < 423$ K. New phenonema include: (i) evidence for a phase transition at *ca* 198 K, indicated by $\{h+1/2, k, 0\}$ superlattice reflections with associated diffuse streaking along the $\langle 100 \rangle$ directions of the tetragonal tungsten-bronze-type subcell; and (ii) a measurable temperature variation of the incommensurate superlattice (ICS) spacing along $\mathbf{k}_{110}$, so that the order parameter increases sharply at *ca* 198 K for decreasing temperature. The unit-cell parameters and space groups of the two component supercells, which intergrow coherently together to give rise to the ICS, have been derived by analysis and computer simulation of the ICS diffraction patterns. Dark-field images of the room-temperature phase revealed a chaotic microdomain texture (~60–100 Å diameter) containing intergrowth defects, and proved that the superstructures have orthorhombic rather than tetragonal symmetry. Structural models are presented, based upon the observed ICS diffraction patterns and dark fields, as well as consideration of the average structure determined previously by X-ray diffraction, and the closely related superstructure of barium sodium niobate (BNN: $Ba_2NaNb_3O_{10}$).

1. Introduction

The physical properties of strontium barium niobate (SBN: $Ba_xSr_{1-x}Nb_2O_6$) have been investigated thoroughly because of some device applications related to its exceptionally large non-linear polarizability (Lines & Glass, 1977). Phase-analysis studies have indicated a structure derived from the tetragonal tungsten-bronze-structure (TTB) type (Jamieson, Abrahams & Bernstein, 1968) for $x < 0.50$, whereas for $x > 0.75$ an orthorhombic derivative was proposed (Carruthers & Grasso, 1970). The ferroelectric/paraelectric Curie temperature ranges from 333 for $x = 0.25$ up to 473 K for $x = 0.75$ (Carruthers & Grasso, 1970; Fig. 5). An incommensurate superlattice (ICS) was first reported by Schneck, Toledano, Whatmore & Ainger (1981) who examined the $(hkl/2)$ reciprocal-lattice plane (tetragonal cell indices; $a = b = 12.3$, $c = 3.91$ Å) using a monochromatic X-ray precession camera. Superlattice spots were found on both bisector directions of the tetragonal cell at positions $\pm(h+[1+\delta]/4, k+[1+\delta]/4, 1/2)$ along [110] [$\delta = 0.26(5)$]. It had been observed previously (Schneck & Denoyer, 1981) that similar behaviour occurred for barium sodium niobate (BNN: $Ba_2NaNb_5O_{15}$) with $\delta = 0.01$ at room temperature, increasing to $\delta = 0.08$–0.12 for $548 < T < 573$ K. For BNN it was established that the ICS was one dimensional (along [110]) by observing variations in intensity of ICS spots along [110] and $[1\bar{1}0]$, consistent with domains having symmetry lower than tetragonal (*e.g.* orthorhombic). For SBN the ISC intensity was identical along these two directions for all samples studied, suggesting a two-dimensional ICS having tetragonal symmetry. It has been proposed that the instability responsible for the ICS in BNN is due to a collective shearing of the $[NbO_6]$ octahedra which constitute the framework of the TTB structure (Schneck, Toledano, Joffrin, Aubree, Joikoff & Babelotaud, 1982). This notion is based upon the room-temperature ($\delta = 0$) structural analysis of Jamieson *et al.* (1968), where O atoms situated in the $Z = 1/2$ plane were split between two positions (see Fig. 8*a* below). However, there are no definitive structural studies of the ICS structures of either SBN or BNN, probably because the superlattice spots are weak and difficult to detect with X-ray or neutron diffraction.

Electron diffraction and high-resolution electron microscope beam-tilting techniques have been used in this laboratory (Bursill & Peng, 1986; Peng & Bursill, 1987) to derive a space group for the commensurate superlattice phase of BNN (*Ibm*2) and a structural model was derived which was consistent with this space group and with the high-resolution images.

Electron diffraction patterns recorded in the temperature range $93 < T \leq 423$ K are hereby presented, which have allowed the reciprocal-lattice geometry of SBN to be more fully explored, owing to the relatively large atomic scattering factors for electrons compared to X-rays. High-resolution dark-field images show that SBN possesses a chaotic microdomain texture consistent with a one-dimensional

0108-7681/87/010049-08$01.50

ICS structure containing two components, each having orthorhombic symmetry. A new phase transition, to a second ICS phase, was discovered at 198 K. Structural mechanisms for the ICS structures are discussed.

2. Experimental

Single-crystal boules of $Ba_{0.5}Sr_{0.5}Nb_2O_6$ were mechanically sliced parallel to (001), (100) and (110), then chemically thinned and polished for electron microscopy by immersion in molten $KHSO_4$ in a Pt crucible at 723–773 K. The washed and dried specimens were then sandwiched between two 75-mesh copper grids. Electron diffraction patterns were recorded for $93 \leq T \leq 423$ K using a JEM-100CX instrument fitted with a Gatan double-tilting heating–cooling goniometer. Beam divergences of $\leq 10^{-4}$ rad were required to obtain sharp diffraction patterns containing weak superlattice reflections. Exposure times of up to 120 s were often required, using Kodak AA Industrex X-ray film. Incommensurate superlattice spacings were measured using a Joyce–Loebl automatic recording densitometer. High-resolution bright- and dark-field images were obtained, at room temperature, using a top-entry goniometer, at 100 kV ($C_s = 0{\cdot}7$ mm) in a JEM 100C instrument fitted with 5, 10, 20 and 40 μm objective apertures.

3. Results

(*a*) [001] *projection*

Figs. 1(*a*), (*b*) show (001) reciprocal-lattice sections from the same area of crystal, at 293 and 173 K respectively. These were selected from a series recorded at 20 K intervals in the range $93 < T \leq 423$ K. Note the superlattice spots $\{h+1/2,\ k+1/2,\ 0\}$ (tetragonal cell indices; $a = b = 12{\cdot}4$, $c = 3{\cdot}91$ Å), which occurred throughout the range $93 < T < 423$ K. These appear strictly commensurate with respect to the strong subcell reflections, at least within our precision of measurement. They increase in intensity, relative to the subcell spots, for decreasing temperatures, and diminish noticeably in intensity at higher temperatures. No splitting of these reflections could be detected. A new set of superlattice reflections, with associated diffuse scattering, appeared suddenly at *ca* 198 K (Fig. 1*b*) at $\{h \div 1/2,\ k,\ 0\}$ symmetrically equivalent positions. This intensity increased continuously, relative to the subcell spots, for temperatures decreasing from 198 to 93 K. The cross-shaped diffuse streaking appearing along the equivalent ⟨110⟩ directions became stronger and sharper in this temperature range. The sharp superlattice reflections appeared strictly commensurate with the subcell spots. Identical results were obtained for sections from two different SBN boules.

(*b*) [110] *projection*

Incommensurate superlattice (ICS) spots were obtained (Fig. 2*a*), corresponding to incommensurability parameter $\delta = 0{\cdot}190$ and $\delta = 0{\cdot}196$ at room temperature, for specimens taken from two different boules of SBN. δ (Fig. 2*b*) is a measure of the deviation of the superlattice spots from the ideal superlattice positions which would occur for a $4 \times d_{110}$ commensurate superstructure. The ICS spots showed increased (decreased) intensity for decreasing (increasing) temperature, and they persisted throughout the temperature range $93 \leq T \leq 423$ K. The variation of δ was measured for our specimen. Fig. 2(*c*) shows an example of a microdensitometer trace used for measurement; the results are given in Fig. 3. δ is nearly constant $[\delta_1 = 0{\cdot}190(5)]$ from 203 up to 423 K, and also constant $[\delta_2 = 0{\cdot}200(5)]$ from 198 to 93 K. A discontinuous increase in δ occurred at *ca* 198 K, coinciding with the appearance of the

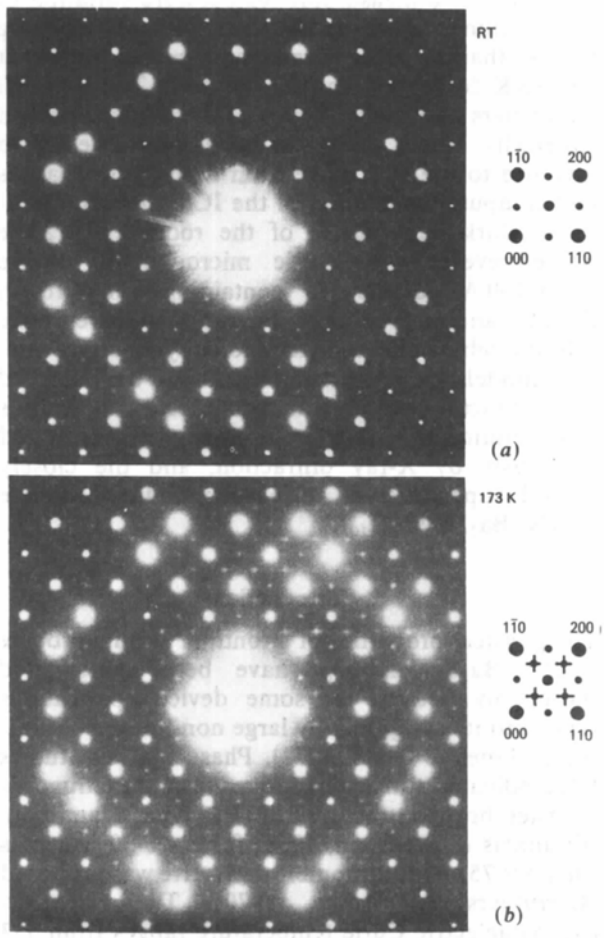

Fig. 1. (001) reciprocal-lattice sections from one area of SBN, at (*a*) 293 K and (*b*) 173 K. Note superlattice spots $\{h+1/2,\ k+1/2,\ 0\}$ for both (*a*) and (*b*). Spots at $\{h+1/2,\ k,\ 0\}$ appear below 198 K, together with cross-shaped diffuse streaking along ⟨110⟩.

additional superlattice spots (and diffuse ⟨110⟩ streaking) in the (001) sections. An almost identical jump in δ occurred for specimens from the second boule. It appears that the transition at 198 K is not of lock-in type. It indicates the existence of two closely related ICS phases, which we will denote δ_1 ($198 \leq T \leq 423$ K) and δ_2 ($93 \leq T \leq 198$ K). Note that we were unable to induce a lock-in transition even by reducing to liquid-nitrogen temperatures, nor were we able to find electron diffraction evidence for the ferroelectric/paraelectric transformation, which should occur at approximately 413 K (for $x = 0{\cdot}50$), according to Carruthers & Grasso (1970). The stoichiometries of our two boules were checked, using X-ray energy dispersive spectroscopy in a JEM 100CX electron microscope. Values obtained ranged from $x = 0{\cdot}50$ to $0{\cdot}55$, confirming the stated as-grown value ($x = 0{\cdot}50$). The Curie temperature may therefore be just beyond the 423 K (nominal) maximum temperature of our goniometer.

For some thinned specimens it proved possible to tilt from [110] to [1$\bar{1}$0] and record a series of reciprocal-lattice sections from the same small (2000 Å diameter) area. Virtually identical ICS patterns were obtained for [110] and [1$\bar{1}$0], with no measurable differences in δ, although the intensity of the superlattice reflections changed relative to that of subcell spots, as expected for the large effective changes in specimen thickness. The ⟨110⟩ zone-axis patterns often showed diffuse streaking along ⟨110⟩ directions and the ICS spots were not, in general, quite as sharp as were the subcell spots for SBN, or as sharp as the corresponding commensurate superlattice spots observed for BNN at room temperature (*cf* Peng & Bursill, 1987). For SBN the ICS spots showed a slight but significant elongation along the corresponding ⟨110⟩ superlattice directions (Fig. 2*a*).

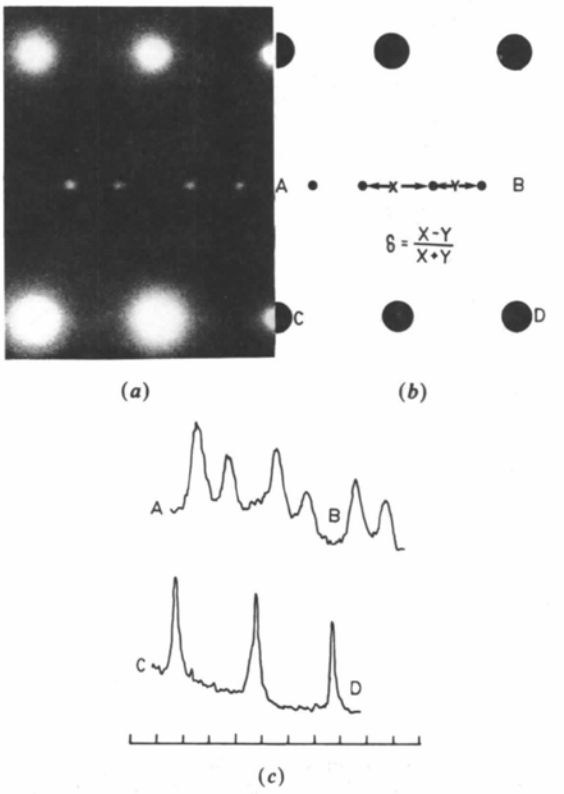

Fig. 2. (*a*) ICS spots ($\delta = 0{\cdot}19$) for [110] projection of SBN lying in rows along [110]. (*b*) Measurements required to determine the ICS incommensurability parameter δ. (*c*) An example of a microdensitometer trace used to measure $\delta(T)$.

(*c*) *Reciprocal lattices for ICS(δ_1) and ICS(δ_2)*

Fig. 4(*a*) gives the reciprocal lattice of the basic TTB-type framework structure (space group *P*4/*mbm*), which is presumably the high-temperature form. Schneck *et al.* (1981) reported that the ICS reflections remained [presumably ICS(δ_1)] up to at least 770 K. From our results for [001] (Fig. 1*a*), [100] (Fig. 5*a*), [110], [11$\bar{1}$] and [11$\bar{2}$] (Figs. 5*b*–*d*) zone-axis patterns, reciprocal-lattice models were constructed (Figs. 4*b*, *c*) for ICS(δ_1) and ICS(δ_2). Note that the presence of both ICS spots and streaking along ⟨110⟩ may give rise to some quite complex diffraction patterns, especially for higher-index zone axes. These provided quite stringent tests for the accuracy of our models. Despite a careful search, we were unable to find any splittings of higher-order subcell (or supercell) reflections, so that any orthorhombic distortion of the subcell parameters must be small. This is consistent with Carruthers & Grasso's (1970) result that the SBN subcell is tetragonal for $x \leq 0{\cdot}50$. Any departure from tetragonality is therefore expected to be very small for our specimens, which had $x = 0{\cdot}50$–$0{\cdot}55$.

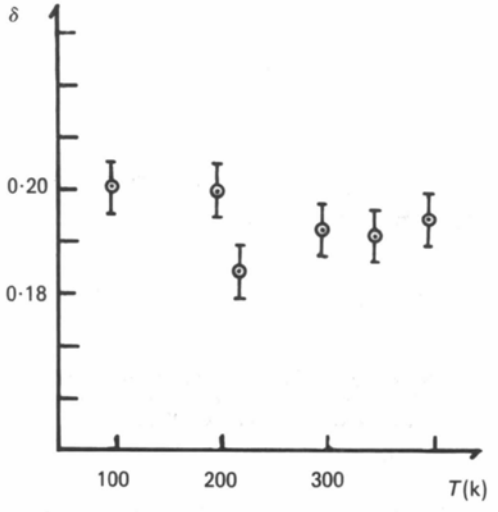

Fig. 3. Variation of $\delta(T)$ for SBN. Note sharp increase of δ on decreasing temperature below 198 K.

(d) Higher-resolution dark-field observations

Use of a 5 μm objective aperture enabled dark-field images to be obtained using pairs of ICS spots for the [110] zone axis. A chaotic microdomain texture was revealed with domain diameters ~60–100 Å. Careful location of the aperture and selection of crystal thickness enabled one-dimensional lattice fringes to be obtained within individual domains (Fig. 6*b*). Note the black fringes within the bright contrast regions. These have spacing of *ca* 18 Å, with occasionally wider spacing of *ca* 27 Å parallel to the (110) lattice planes. Thus they represent 2× and 3× multiples of the 8·8 Å framework spacings. The absence of such fringes in the dark-contrast areas of Fig. 6(*b*) implied that the superstructure is in fact one dimensional, consisting of two orientation variants, one parallel to **k**(110), having the long axis lying in the plane of observation, and one parallel to **k**(1$\bar{1}$0), having the long axis lying parallel to the electron beam. These dark-field observations clearly require an orthorhombic rather than tetragonal superstructure for ICS(δ_1). We have not yet been able to record higher-resolution images of the ICS(δ_2) phase (below 198 K). Note that the extent of superstructure visible is severely limited, being (4–8) × 18 Å, typically containing only one wider spacing per domain. Use of a 10 μm objective aperture, so that, for example, two subcell reflections and the adjacent superstructure reflections showed, in the case of the thinnest crystalline areas only, some modulation of the 8·89 Å subcell fringes (Fig. 6*c*). This is consistent with the preceding observations (Figs. 5*a*,*b*) in that the modulation is restricted to areas of 60–100 Å diameter. However, domains are no longer visible owing to the overwhelmingly large contribution to the background fringe contrast coming from the subcell. If four or more subcell reflections were included in the largest aperture (indicated in Fig. 2*a*) then it was not possible to find any evidence in the image for the ICS superstructure, again owing presumably to the overwhelmingly large contributions from the subcell reflections.

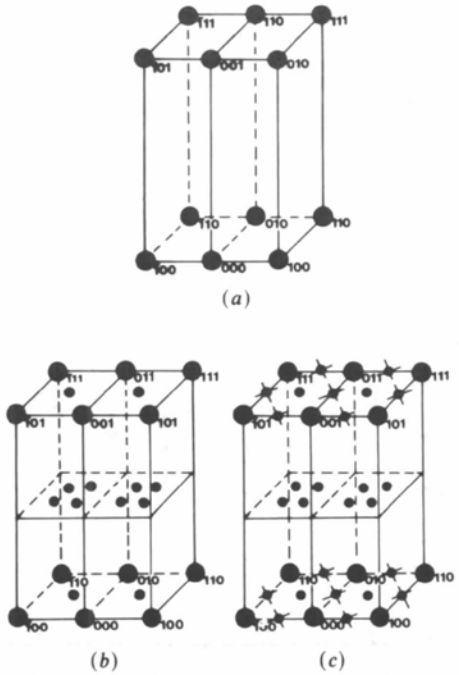

Fig. 4. (*a*) Reciprocal lattice of TTB-type framework (space group *P4/mbm*). (*b*), (*c*) Reciprocal-lattice models for the room-temperature (δ_1) and low-temperature (δ_2) ICS structures.

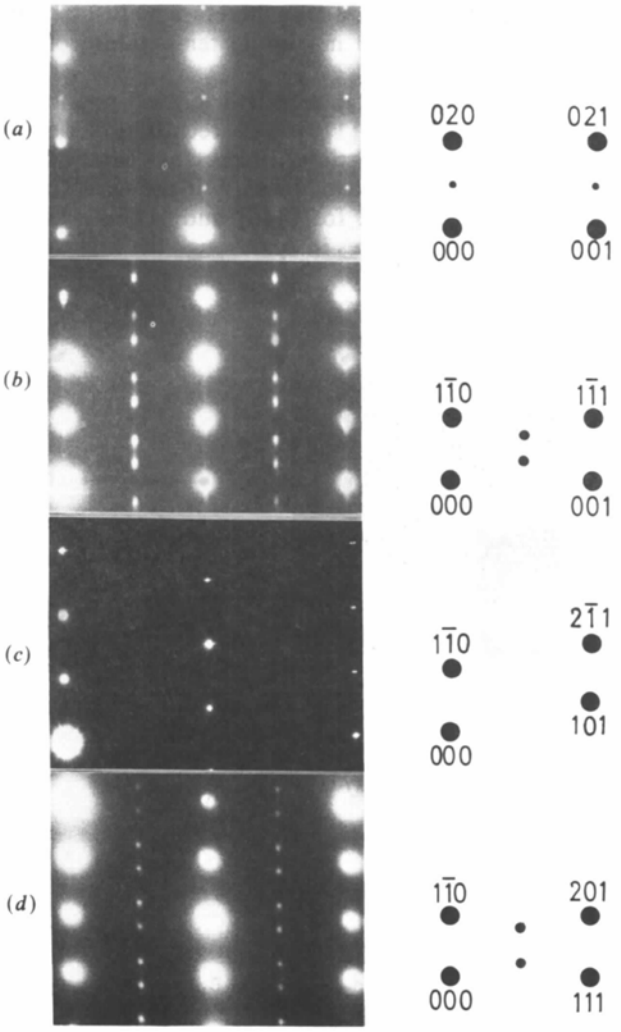

Fig. 5. Reciprocal-lattice sections of SBN for (*a*) [100], (*b*) [110], (*c*) [11$\bar{1}$] and (*d*) [11$\bar{2}$]. (*a*) and (*b*) are related by a tilt of 45° and [001] whereas (*b*), (*c*) and (*d*) are a series related by tilting about [1$\bar{1}$0]. Note the absence of superlattice spots for (*c*) and different dispositions of incommensurate superlattice spots in (*b*) and (*d*).

4. Discussion

(*a*) *Unit-cell geometry*

The dark-field observations (Figs. 6*a*,*b*) clearly demand the existence of two one-dimensional orientational variants of ICS(δ_1). Figs. 7(*a*), (*b*) show how the observed ICS(δ_1) reciprocal lattice may be decomposed into two such variants, with long axes parallel to [110] and [1$\bar{1}$0] of the tetragonal subcell. Note that the $l = 0, 2$ levels are identical for these two. The indices were assigned using the orthorhombic unit cell $a_o = 17{\cdot}58$, $b_o = 35{\cdot}16$, $c_o = 7{\cdot}83$ Å. This assumes that $\delta = 0$, a commensurate superlattice having multiplicity $4 \times d_{110}$. In fact, the ICS(δ_1) may be regarded as an intergrowth structure containing slabs of this unit cell, of infinite extent parallel to $(010)_o$, uniformly mixed (Fujiwara, 1957) with slabs having a unit cell half as wide along $\mathbf{b}_o$. Thus, computer simulations of the ICS diffraction pattern, using the theory and computer programs developed by Grzinic (1983, 1985), show the observed value $\delta_1 = 0{\cdot}195$ corresponds to a mixing ratio (R) of approximately 0·75 for these two components. Fig. 8 gives a computer simulation of the ICS diffraction pattern, showing the variation of spot positions with mixing ratio. Note the ICS spots remain quite sharp for $0{\cdot}25 \leq R \leq 1{\cdot}0$. The end member ($R = 1$) corresponds to unit cell $a_o = 17{\cdot}58$, $b_o = 35{\cdot}16$ and $c_o = 7{\cdot}83$ Å.

The other end member ($R = 0$) corresponds to an orthorhombic unit cell $a'_o = 17{\cdot}58$, $b'_o = 17{\cdot}58$, $c'_o = 7{\cdot}83$ Å, and thus corresponds geometrically to the unit cell used by Jamieson, Abrahams & Bernstein (1969) for their refinement of BNN. This result is also consistent with the high-resolution dark-field images of Figs. 6(*b*), (*c*), as will be demonstrated below after structural models are introduced. Fig. 7(*c*) shows a reciprocal-lattice model deduced for the smaller orthorhombic unit cell (a'_o, b'_o, c'_o), $b'_o = 1/2b_o$.

(*b*) *Space-group assignments*

Earlier attempts to use space group *P*4*mbm* or *P*4*b*2 (Francombe, 1960) or *P*4*bm* (Jamieson *et al.*, 1968) assumed the 12·43 × 12·43 × 3·915 Å tetragonal subcell. The observed extinction conditions: *hkl*, $h + l = n$; *hk*0, $h = 2n$; *h*0*l*, $h + l = 2n$; 0*kl*, *k*, $l = 2n$; *h*0*l*, $h = 2n$; 0*k*0, $k = 2n$; 00*l*, $l = 2n$; applied to the (a_o, b_o, c_o) unit cell deduced above lead to two possible orthorhombic space groups, *Bbm*2 and *Bmm*2. Neither possess an inversion center, and both are consistent with known ferroelectricity of SBN at room temperature. Placement of the symmetry elements of *Bbm*2 and *Bmm*2 onto the *x*-axis projection of the average structure of SBN (Jamieson *et al.*, 1968; Fig. 3) reveals quickly that only *Bmm*2 is compatible with this structure, regardless of the choice of different possible alignments of a_o, b_o axes with respect to the

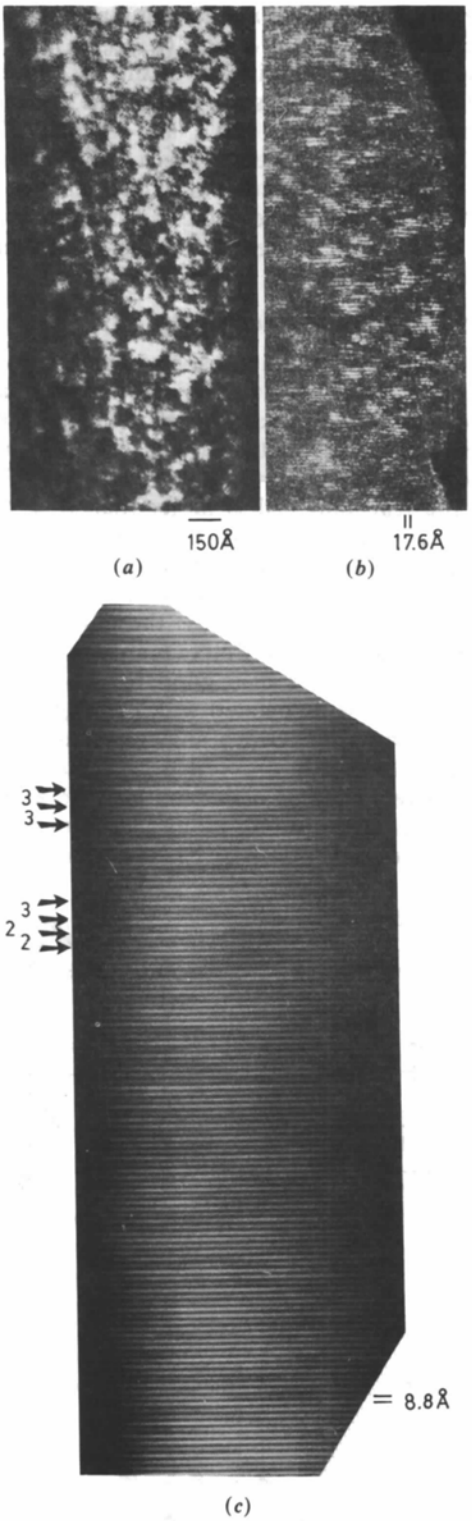

Fig. 6. (*a*) Dark-field image of SBN showing chaotic domain texture on 100 Å scale. (*b*) (110) lattice fringes within bright domains; 18 Å spacings predominate but 27 Å fringes sometimes intergrow. (*c*) Effect of including subcell reflections in the image, some contrast variations are still apparent, indicating intergrowth defects, but 8·8 Å subcell spacings now predominate.

symmetry elements. *Bmm*2 is left as a reasonable choice for the space group of (a_o, b_o, c_o).

The extinction conditions for the (a'_o, b'_o, c'_o) unit cell (Fig. 7*c*) are consistent with the orthorhomic space groups *Cmm*2, $Cm2_1$ and *Bbm*2. Of these, *Bbm*2 may be eliminated since it is not compatible with the average structure of SBN, leaving *Cmm*2 and $Cm2_1$ as reaonable choices of space groups for (a'_o, b'_o, c'_o). Both of these lack a center of symmetry.

(*c*) *X-ray structure refinement of SBN*

This is shown in Fig. 9. Labels refer to sites having different atomic nature and point symmetries, according to atomic coordinates given by Jamieson *et al.* (1968). That refinement used space group *P*4*bm*, with unit-cell parameters $a = 12{\cdot}43$, $b = 12{\cdot}43$, $c = 3{\cdot}915$ Å. That the true unit cell is larger than this, actually $(a_o, b_o, c_o) + (a'_o, b'_o, c'_o)$ in the ratio 3:1 as shown above, is indicated by the apparent disorder for atoms with $z = 0{\cdot}5$. Thus the O-atom sites Ox(4) and Ox(5) have 50% occupancies across the mirror planes. It was suggested later, for BNN (Jamieson *et al.*, 1969), but the argument is also good for SBN, that this disorder may be associated with $[NbO_6]$ octahedra, so that along **c** Nb–O–Nb angles are reduced from 180 to ~165°. An ordered arrangement of such cooperatively sheared octahedra leads to a doubling of the *c* axis. The O atoms around Ba form a distorted tricapped trigonal prism, Sr has distorted cuboctahedral coordination. No site splittings were detected for Ba, Sr or Nb sites. This situation is different from that for BNN, where there are significant splittings of Ba sites (Jamieson *et al.*, 1969), and is consistent with our electron diffraction results, where the superlattice reflections for SBN were very significantly weaker than was the case for BNN.

All of the metal atoms in SBN are displaced along **c** from the nearest mean plane of O atoms, in the same sense, which provides the origin of ferroelectricity and determines the macroscopic polarity. The ferroelectric properties seem to be determined primarily by the Nb^{5+} displacements with respect to these oxygen planes (Jamieson *et al.*, 1968; Fig. 1).

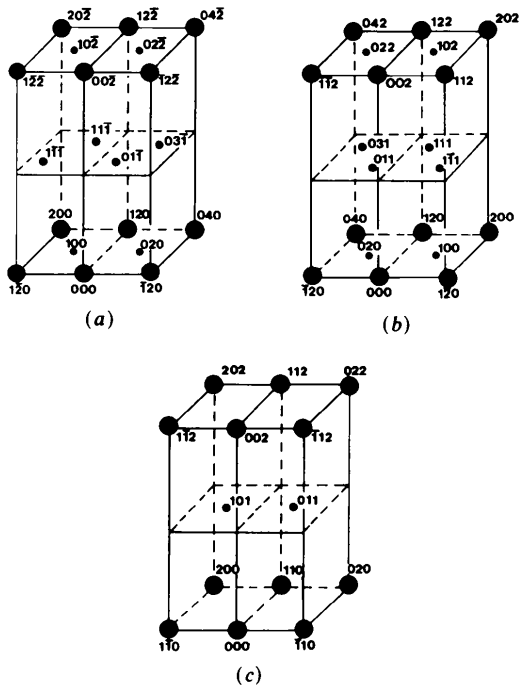

Fig. 7. (*a*), (*b*) Two orientation variants of ICS(δ_1), indices were assigned using orthorhombic cell $a_o = 17{\cdot}58$, $b_o = 35{\cdot}16$ and $c_o = 7{\cdot}83$ Å, assuming a $4 \times d_{110}$ commensurate superlattice. (*c*) Reciprocal-lattice model for (a'_o, b'_o, c'_o), $b'_o = 1/2b_o$, unit cell.

(*d*) *Superstructure of BNN*

It has been shown that a reasonable space group for BNN is *Ibm*2, with orthorhombic cell parameters $a''_o = 35{\cdot}18$, $b''_o = 35{\cdot}24$ and $c''_o = 7{\cdot}998$ Å (Peng & Bursill, 1987). The structural model derived, on the basis of high-resolution dark-field images of the

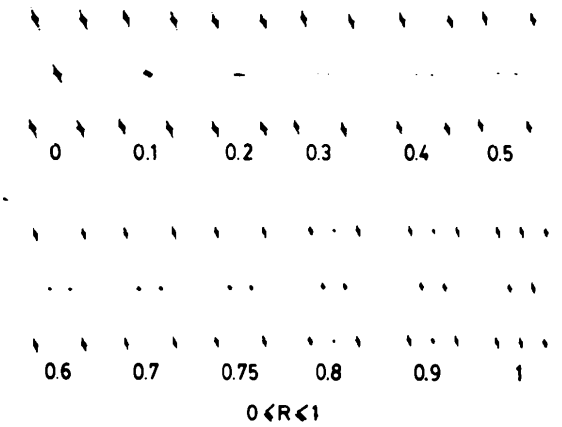

Fig. 8. Computer simulation of the variation of the ICS(δ_1) spot positions with mixing ratio of two components, corresponding to end members (a_o, b_o, c_o) and (a'_o, b'_o, c'_o) where $b_o = 2b'_o$. The observed $\delta = 0{\cdot}195$ corresponds to the ratio 0·75.

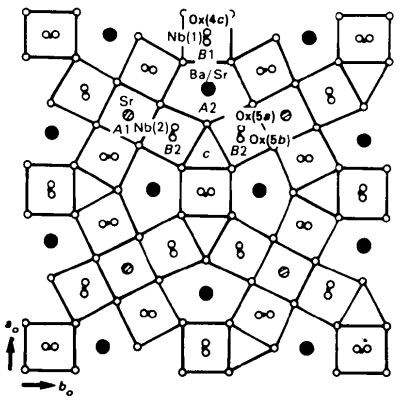

Fig. 9. [001] projection of $Ba_xSr_{1-x}Nb_2O_6$ (after Jamieson *et al.*, 1968). Note location of split O-atom sites Ox(4), Ox(5*a*, 5*b*).

superstructure and image matching, is given here as Fig. 10(*a*). Note the concerted clockwise (*C*) and anticlockwise (*A*) displacements of O atoms having sequence *CAAC*... along $[010]''_o$, *CACA*... along $[100]''_o$ and *CA*... along $[001]''_o$, giving slightly distorted cuboctahedral coordination for Sr. There are also ordered displacements of Na ions along $[010]''_o$, required for image matching. In addition, two O-atom sites remain undetermined, one [labelled Ox(4)] was assumed to be ordered, with displacements antiparallel to the adjacent Ba ions, whilst the other [labelled Ox(5)] was assumed to remain disordered at room temperature. Ordering of these sites, midway between two undisplaced Ba sites, may give rise to a further phase transition, observed in BNN at 113 K. It should be noted that neither Ox(4) or Ox(5) displacements could be detected in the electron diffraction or high-resolution study, owing to their relatively very weak diffraction effect, compared with those of the Ba displacements.

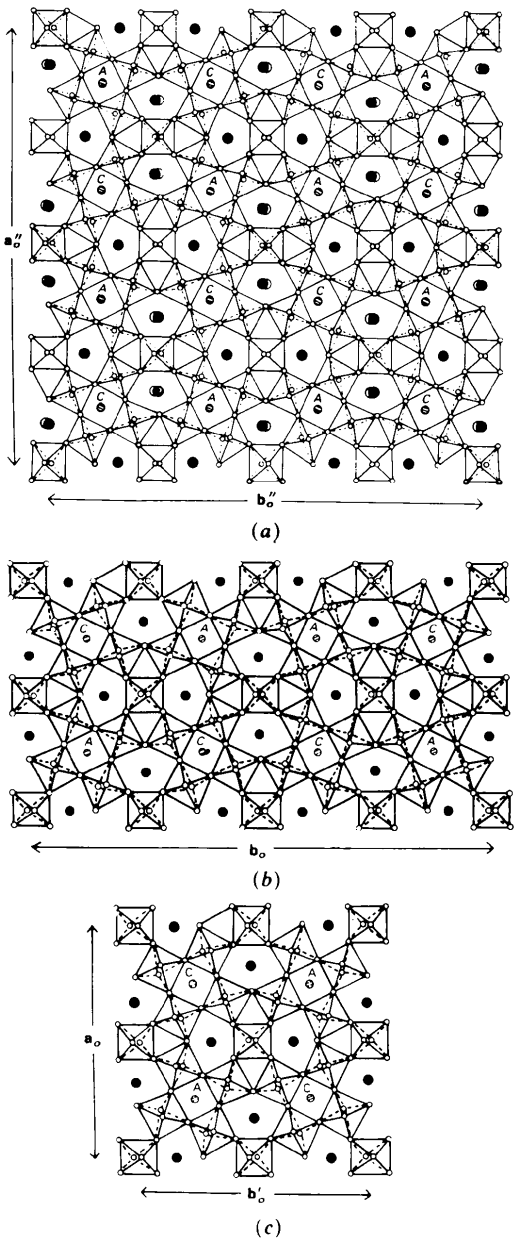

Fig. 10. (*a*) Superstructure of BNN (after Peng & Bursill, 1987) showing displacements of Ba and O atoms. Note concerted rotations of Ox(7, 8) atoms and ordering of Ox(4) sites along [010]. Note that $a''_o = 2a_o = 2a'_o$. (*b*) Superstructure model for (a_o, b_o, c_o) component of ICS(δ_1), assuming space group *Bmm*2 and structural relationship to (*a*). Note sequence of concerted rotations of O atoms represented by *CAAC* along $\mathbf{b}_o$ and *CA*... along both $\mathbf{a}_o$ and $\mathbf{c}_o$. (*c*) Superstructure model for (a'_o, b'_o, c'_o) component of ICS(δ_1), assuming space group *Cmm*2. Note sequence of concerted rotations of O atoms, represented by *CA*... along $\mathbf{a}'_o$, $\mathbf{b}'_o$ and $\mathbf{c}'_o$.

(*e*) *Models for incommensurate superstructure of SBN at room temperature*

Comparison of the unit cells and space groups deduced above for SBN, with the model for BNN, and consideration of the average structure deduced for SBN by Jamieson *et al.* (Fig. 8) leads immediately to the structural models shown in Figs. 10(*b*), (*c*) for $(\mathbf{a}_o, \mathbf{b}_o, \mathbf{c}_o)$ and $(\mathbf{a}'_o, \mathbf{b}'_o, \mathbf{c}'_o)$ respectively. Since there are no displacements of Ba atoms, it is no longer necessary to retain a doubled $\mathbf{b}_o$ (or $\mathbf{b}'_o$) axis, leaving sequence *CA*... along both $[001]_o$ (or $[001]'_o$) and $[100]_o$ (or $[100]'_o$). $(\mathbf{a}_o, \mathbf{b}_o, \mathbf{c}_o)$ and $(\mathbf{a}'_o, \mathbf{b}'_o, \mathbf{c}'_o)$ then differ only in that $\mathbf{b}_o = 2\mathbf{b}'_o$, which may readily be achieved by taking sequence *CAAC*... for b_o and *CA*... for b'_o. Thus the two cells have a common structural principle consisting of the concerted rotational orderings of Ox(7) and Ox(8) sites along a_o and c_o axes. The question of possible orderings of Ox(4) and Ox(5) sites cannot be determined on the basis of our present results. These could both remain disordered and still be consistent with space groups *Bmm*2 and *Cmm*2, respectively; or one half of these sites could become ordered (indicated in Figs. 10*b*,*c*). It seems reasonable to suggest that at least one of these O-atom sites is disordered at room temperature, leaving the way open for a further transition at 198 K (observed above). Of course the latter may also involve some displacements of Ba atoms, similar to that which occurs in BNN.

The origin of the incommensurate superlattice structure of SBN then appears to lie in the existence of two competing structures $(\mathbf{a}_o, \mathbf{b}_o, \mathbf{c}_o)$ and $(\mathbf{a}'_o, \mathbf{b}'_o, \mathbf{c}'_o)$ which are very closely related and presumably have almost identical energies. Although no static Ba displacements were detected by Jamieson *et al.* (1968) they did report significant anisotropic thermal parameters for some Ba atoms. This would presumably favor some stabilization of the doubled b_o-axis component of the incommensurate structure. Note that the pseudo-tetragonal nature of the SBN superstructure arises presumably due to the absence

of static Ba-atom displacements. The latter would tend to lead to the different a and b subcell dimensions. The concerted O-atom rotations C and A, which are symmetrically placed with respect to both a and b, will not induce a departure from tetragonality. Thus only the small possible shifts of Ox(4) or Ox(5) would remain to induce different a and b subcell dimensions.

Our analysis of the incommensurate superlattice patterns (see results in Fig. 8) required that the slab widths for the intergrowths were actually 8·8 and 17·6 Å, requiring use of primitive cells for the intergrowth slabs. Fig. 11 shows the corresponding [110] projection of the incommensurate superstructure. Thus the sequence of concerted rotations along $\mathbf{b}_o$ (or $\mathbf{b}'_o$) was found to be a mixture of (CA), (AC), (C) and (A) units rather than of $(CAAC)$ and (CA) units. A typical sequence might be $(CA)(A)(CA)(C)$-$(AC)(A)(CA)(C)\ldots$. Such sequences are quite consistent with the contrasts shown by the high-resolution dark-field images (Figs. 7*b*,*c*). Further detailed explanation of these results, and an application of Grzinic's theory to the superstructures existing below 198 K, must be left for a later paper (Grzinic, Peng & Burstill, in preparation).

5. Concluding remarks

The present results again emphasize that very significant information may be obtained by electron diffraction, when weak symmetry elements develop in a framework structure owing to a series of structural phase transitions. Thus the reciprocal-lattice geometry may be determined more readily than is the case using X-ray or neutron diffraction alone. Again the presence of small (100 Å diameter) domains of an orthorhombic superstructure, giving an appearance overall of pseudotetragonal symmetry, could only be detected using high-resolution dark-field imaging techniques, since there is no measurable change in subcell parameters which would otherwise have indicated a low symmetry.

The present structural models should be regarded as tentative, since we are not yet able to obtain quantitative measurements of superlattice reflections, and fully test the models. Even the high-resolution images were not very sensitive to the superstructure, yielding only just sufficient information to confirm the true orthorhombic nature of the superstructure. Nevertheless, we believe that our structural models, which are certainly based upon the average structure determinations by X-ray diffraction and space groups derived from electron diffraction, should provide a reasonable basis for future definitive X-ray or neutron diffraction work. It should now be possible to devise suitable experiments for these techniques, to allow quantitative testing of the models and further study, using inelastic neutron scattering perhaps, of the series of structural phase transitions exhibited by both SBN and BNN.

This work was supported by the Australian Research Grants Committee and the University of Melbourne. Peng Ju Lin is grateful to the Education Department of the People's Republic of China for permission to visit Melbourne. The authors express their appreciation to Mr P. Hanan (University of Melbourne) for recording the microdensitometer traces and Dr P. Self (University of Melbourne) for help with the XEDS analysis of our specimens. The support of the Facility for High Resolution Electron Microscopy, Arizona State University (National Science Foundation grant No. DMR-8306501), during the preparation of this paper, is gratefully acknowledged.

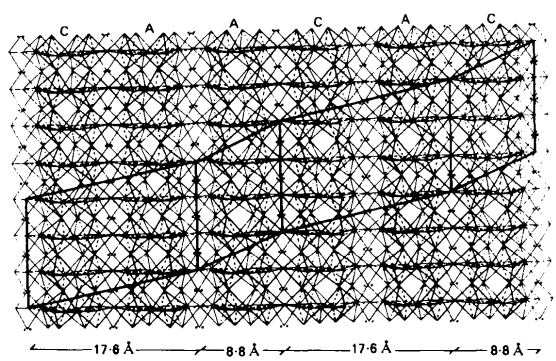

Fig. 11. [110] projection of incommensurate superstructure (δ_1) showing intergrowth of primitive unit cells, corresponding to half-width slabs of (a_o, b_o, c_o) and (a'_o, b'_o, c'_o), as required for computer matching of ICS(δ_1) diffraction patterns. Note the mechanism of coherent intergrowth of these components.

References

BURSILL, L. A. & PENG JU LIN (1986). *Philos. Mag.* A. In the press.
CARRUTHERS, J. R. & GRASSO, M. (1970). *J. Electrochem. Soc.* **117**, 1426-1430.
FRANCOMBE, M. H. (1960). *Acta Cryst.* **12**, 131-140.
FUJIWARA, K. (1957). *J. Phys. Soc. Jpn*, **12**, 7-13.
GRZINIC, G. (1983). PhD thesis, Univ. of Melbourne.
GRZINIC, G. (1985). *Philos. Mag.* **52**, 161-187.
JAMIESON, P. B., ABRAHAMS, S. C. & BERNSTEIN, J. L. (1968). *J. Chem. Phys.* **48**, 5048-5057.
JAMIESON, P. B., ABRAHAMS, S. C. & BERNSTEIN, J. L. (1969). *J. Chem. Phys.* **49**, 4352-4363.
LINES, M. E. & GLASS, A. M. (1977). *Principles and Applications of Ferroelectrics and Related Materials.* Oxford: Clarendon Press.
PENG JU LIN & BURSILL, L. A. (1987). *Acta Cryst.* B. Submitted.
SCHNECK, J. & DENOYER, F. (1981). *Phys. Rev. B*, **23**, 383-388.
SCHNECK, J., TOLEDANO, J. C., JOFFRIN, C., AUBREE, J., JOIKOFF, B. & BABELOTAUD, A. (1982). *Phys. Rev. B*, **25**, 1766-1785.
SCHNECK, J., TOLEDANO, J. C., WHATMORE, R. & AINGER, F. W. (1981). *Ferroelectrics*, **36**, 327-329.